



Title	Thermoelectric Properties of Solution Combustion Synthesized Al-Doped ZnO
Author(s)	Zhang, Lihua; Tosho, Tsuyoshi; Okinaka, Noriyuki; Akiyama, Tomohiro
Citation	MATERIALS TRANSACTIONS, 49(12), 2868-2874 https://doi.org/10.2320/matertrans.MAW200801
Issue Date	2008-12-01
Doc URL	http://hdl.handle.net/2115/77069
Type	article
File Information	Mater. Trans. 49(12) 2868.pdf



[Instructions for use](#)

Thermoelectric Properties of Solution Combustion Synthesized Al-Doped ZnO

Lihua Zhang*, Tsuyoshi Tosho, Noriyuki Okinaka and Tomohiro Akiyama

Center for Advanced Research of Energy Conversion Materials, Hokkaido University, Sapporo 060-8628, Japan

Thermoelectric properties of Al-doped ZnO prepared by solution combustion synthesis using urea as fuel and sintered by spark plasma sintering were investigated for developing an energy- and time-saving synthesis method to decrease its thermal conductivity without a significant deterioration in other thermoelectric properties. The desired materials were successfully synthesized and sintered. The thermoelectric properties of the synthesized products subjected to planetary ball milling (PBM) treatment before sintering were compared with those of synthesized products not subjected to PBM treatment; the results showed that the former products had a larger power factor and higher thermal conductivity than the latter products. The thermal conductivity of all as-synthesized products was in the range of $8.3\text{--}19.7\text{ W}\cdot\text{m}^{-1}\cdot\text{K}^{-1}$ at room temperature, which was significantly lower than that of the products synthesized by a conventional solid-state reaction method. $(\text{Zn}_{0.99}\text{Al}_{0.01})\text{O}$ obtained by PBM had the highest dimensionless figure of merit ZT of 0.050 at 863 K. From these results, it is inferred that solution combustion synthesis is an effective method for synthesizing Al-doped ZnO with relatively low thermal conductivity for high-temperature thermoelectric applications. [doi:10.2320/matertrans.MAW200801]

(Received April 14, 2008; Accepted September 16, 2008; Published October 29, 2008)

Keywords: thermoelectric materials, zinc oxide, solution combustion synthesis, planetary ball milling, thermal conductivity

1. Introduction

Recently, thermoelectric materials, which can be used to directly convert thermal energy into electricity (Seebeck effect) and vice versa (Peltier effect), have been intensively researched because of their applicability in thermoelectric generation and cooling/heating.¹⁾ To develop thermoelectric materials for high-temperature applications, considerable attention has been focused on oxides, which have high resistance against oxidation and are thermodynamically stable at high temperature.²⁻⁷⁾ Among the reported oxide thermoelectric materials, *n*-type ZnO-based material^{8,9)} has been reported to have a high dimensionless figure of merit ZT , which is generally used to evaluate thermoelectric properties and is defined as

$$ZT = T\alpha^2\sigma/\kappa \quad (1)$$

where T , α , σ , and κ are the absolute temperature, Seebeck coefficient, electrical conductivity, and thermal conductivity, respectively. $\alpha^2\sigma$ is known as the power factor (PF) of thermoelectric material, and it is determined solely by the electron transport properties of the material.

ZnO is a versatile material used in several commercial applications such as transparent electrodes, piezoelectric devices, varistors, and surface acoustic waves (SAW) devices. It is a good conductive oxide with a wide forbidden bandgap. ZnO was first identified as a potential candidate for practical thermoelectric applications by Ohtaki *et al.*,⁸⁾ because of its figure of merit $ZT\sim 0.3$ at 1273 K when it is doped with a small amount of Al. Subsequently, many researches on the thermoelectric properties of ZnO-based materials were conducted, where several elements such as Ti, Ni, Mg, Sn, or Al were doped in the Zn-site. Among the doped ZnO samples reported thus far, Al-doped ZnO exhibited the highest ZT value.⁹⁻¹⁷⁾ A relatively high thermal conductivity within the range of $20\text{--}40\text{ W}\cdot\text{m}^{-1}\cdot\text{K}^{-1}$ at room temperature, generally observed in doped ZnO samples,

prevents us from obtaining a considerably large ZT value. Therefore, it is very important to decrease the lattice thermal conductivity of ZnO-based materials for thermoelectric applications.

Ohtaki *et al.*⁹⁾ synthesized Al-doped ZnO with a nanovoid structure by using combustible nanosized polymer particles as void-forming agents via a solid-state reaction process; the result showed that the thermal conductivity of Al-doped ZnO was in the range of $17\text{--}31\text{ W}\cdot\text{m}^{-1}\cdot\text{K}^{-1}$ at room temperature, which was lower than that of the samples synthesized by a conventional solid-state reaction method. However, the thermal conductivity of Al-doped ZnO was still not sufficient for thermoelectric applications. The reported procedure to introduce homogeneously distributed nanovoids in ZnO ceramics is very complex to be used in the synthesis of practical thermoelectric materials. Furthermore, solid-state reaction method is time and energy consuming since the materials used in it are usually ground and calcined several times to obtain a high-purity product. Therefore, it is very important to develop a relatively easy method to reduce the thermal conductivity of ZnO-based thermoelectric materials.

Cai *et al.* studied the thermoelectric properties of Al-doped ZnO consisting of fine particles using a sol-gel process in which zinc acetate was used as one of the starting materials. Notably, the resulting samples exhibited a low thermal conductivity in the range of $22\text{--}27\text{ W}\cdot\text{m}^{-1}\cdot\text{K}^{-1}$ at room temperature, which is definitely lower than those reported for sintered ceramics. This indicates that solution processes are most likely to reduce the thermal conductivity of ZnO ceramics because they form fine particles in the ceramics.¹⁸⁾

Therefore, in this study, we employed a "solution combustion synthesis" (SCS)^{19,20)} method since it is considered as one of the most simple solution-based combustion synthesis methods. Notably, the chemical energy released from the redox reaction instantaneously heats up the system, and neither additional heating nor special chemicals are required. Thus, the SCS method is considered to be one of the easiest energy-saving methods to produce ceramics

*Graduate Student, Hokkaido University

consisting of fine particles. By measuring the thermoelectric properties obtained by the SCS method, we discussed the possibility of this method as one of the most effective methods to produce thermoelectric materials possessing a low thermal conductivity.

2. Experimental Procedure

Polycrystalline Al-doped ZnO ($(\text{Zn}_{1-x}\text{Al}_x)\text{O}$ ($x = 0.005, 0.01, 0.02$)) was prepared from the raw materials of metal nitrates $\text{Zn}(\text{NO}_3)_2 \cdot 6\text{H}_2\text{O}$ (99.0 mass% purity, Kanto Chemical, Tokyo, Japan) and $\text{Al}(\text{NO}_3)_3 \cdot 9\text{H}_2\text{O}$ (98.0 mass% purity, Kanto Chemical, Tokyo, Japan). Stoichiometric amounts of the metal nitrates were dissolved in distilled water, and an appropriate amount of $\text{CO}(\text{NH}_2)_2$ (99.0 mass% purity, Kanto Chemical, Tokyo, Japan) was added to the solution. Then, the mixture was electromagnetically stirred at 353 K to obtain a homogeneous solution. Next, the solution was poured into an Al_2O_3 crucible, and the crucible was placed in a muffle furnace and rapidly heated to 623 K in air. The self-propagating process of smoldering-type combustion occurred and completed within several minutes. After the synthesis of Al-doped ZnO, the colorless solution turned into pink porous bulk; this bulk was ground into powder using a carnelian mortar and pestle, and then some powders were milled by planetary ball milling (PBM) (Pulverisette-6, Fritsch, Idar-Oberstein, Germany) at 200 rpm for 10–100 min to obtain fine powders. The obtained powders were sintered using a graphite die into pellets with a diameter of 10 mm by spark plasma sintering (SPS) (SPS-511S, Sumitomo Coal Mining, Tokyo, Japan) under vacuum conditions under a pressure of 38 MPa for 3–15 min. The sintering temperature was controlled to be within the range of 973–1193 K to avoid the reduction of the product by carbon foil. In this paper, the spark plasma sintered samples subjected to PBM treatment before sintering are denoted as “PBMed” samples, and the samples that are synthesized without PBM treatment are denoted as “no PBM” samples.

The synthesized samples were characterized by X-ray diffraction analysis (Miniflex, Rigaku, Tokyo, Japan) using $\text{CuK}\alpha_1$ radiation. The morphology of the samples was observed by a scanning electron microscope (SEM) (JSM-7000F, JEOL, Tokyo, Japan), and the distribution of Al in the samples was observed by the mapping images of an energy dispersive X-ray spectroscopy (EDS) analysis. The particle

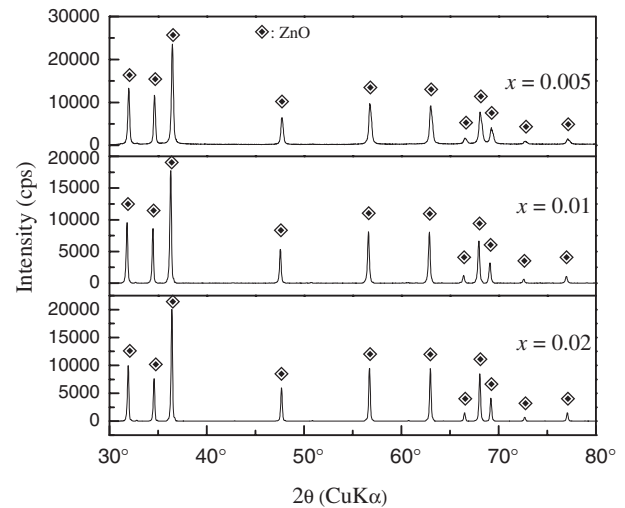


Fig. 1 X-ray diffraction patterns of SCSed powders of $(\text{Zn}_{1-x}\text{Al}_x)\text{O}$ doped with different amounts of Al ($x = 0.005, 0.01, 0.02$).

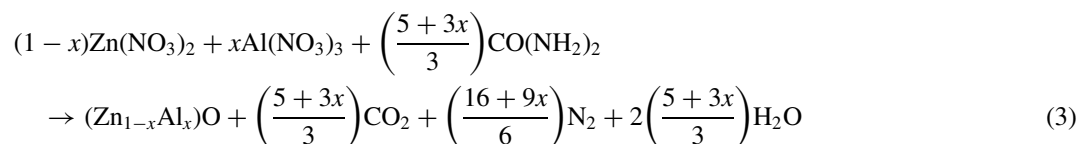
size distribution of powders with different PBM times was measured by a particle size distribution analyzer (LA-950, Horiba, Kyoto, Japan). The electrical conductivity and Seebeck coefficient were simultaneously measured using a Seebeck coefficient/electric resistance measuring system (ZEM-2, Ulvac-Rico, Yokohama, Japan) from room temperature to 865 K. For the measurement of thermal diffusivity and heat capacity, disk specimens with a diameter of 10 mm and thickness of 1–2 mm were cut from the sintered samples. The disks were coated with black carbon to increase the amount of energy absorbed. The thermal diffusivity and heat capacity of the samples were measured using a laser flash thermal constant analyzer (TC-7000, Ulvac-Riko, Yokohama, Japan); their densities were measured by the Archimedes method. The thermal conductivity κ was calculated as

$$\kappa = DC_p d \quad (2)$$

where D , C_p , and d are the thermal diffusivity, heat capacity, and experimental density, respectively.

3. Results and Discussion

The theoretical stoichiometric equations for the formation of $(\text{Zn}_{1-x}\text{Al}_x)\text{O}$ can be written as follows:



The metal nitrates in the raw materials acted as oxidizing agents in the reaction; urea $\text{CO}(\text{NH}_2)_2$ acted as fuel, and it was oxidized by nitrate ions during the process. During synthesis, a large amount of reaction heat was released rapidly, which resulted in the release of CO_2 , N_2 , and H_2O as gaseous products. Equation (3) showed that more than 7 mol of gases were released for the production of 1 mol Al-doped ZnO, which resulted in its porous structure.

Figure 1 shows the X-ray diffraction patterns of SCSed powders doped with different amounts of Al. All the peaks correspond to ZnO (JCPDS-ICDD 36-1451); impurity peaks were not detected. According to the analyses results of the particle size distributions of the powders milled for different times by the PBM process, it was observed that the average particle size decreased with milling time, from 4 μm before milling to 1–2 μm after milling for 100 min. When the milling

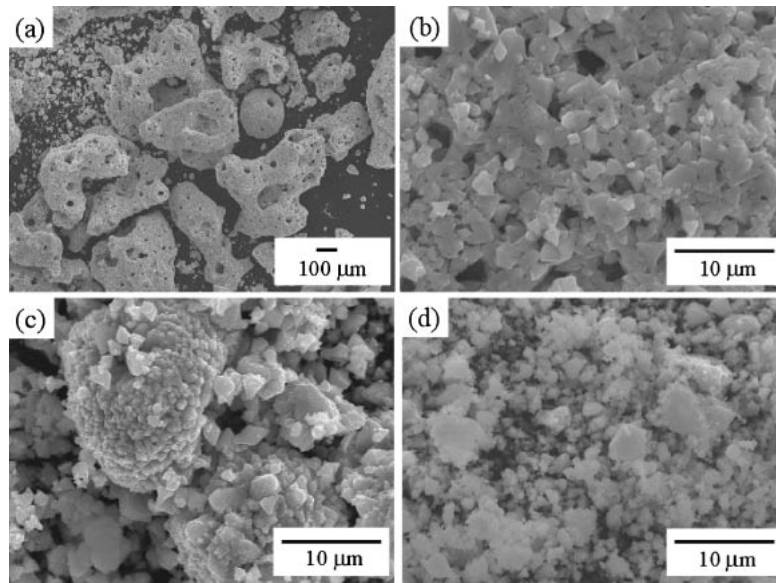


Fig. 2 SEM images of SCSed powder of $(\text{Zn}_{0.99}\text{Al}_{0.01})\text{O}$ sample. (a) and (b) samples directly after SCS; (c) powder of the SCSed sample ground using carnelian mortar and pestle; and (d) the powder obtained after PBM.

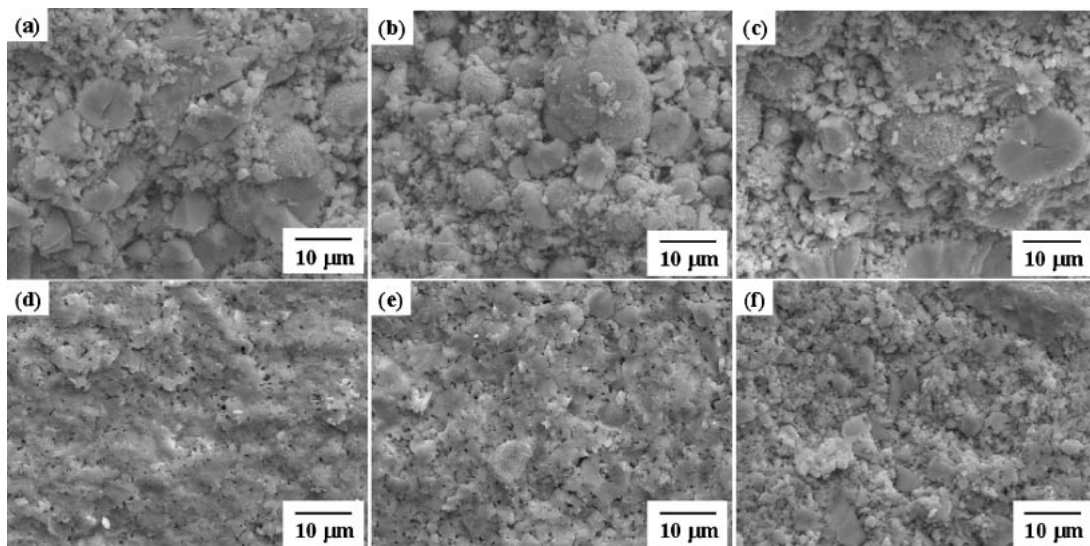


Fig. 3 SEM cross-section images of PBMed and no PBM samples of $(\text{Zn}_{1-x}\text{Al}_x)\text{O}$ ($x = 0.005, 0.01, 0.02$) after spark plasma sintering. (a) $x = 0.005$, no PBM; (b) $x = 0.01$, no PBM; (c) $x = 0.02$, no PBM; (d) $x = 0.005$, PBMed; (e) $x = 0.01$, PBMed; and (f) $x = 0.02$, PBMed.

time was longer than 100 min, the average particle size had almost no change. Therefore, in the PBM process before sintering, the milling time was selected to be 100 min.

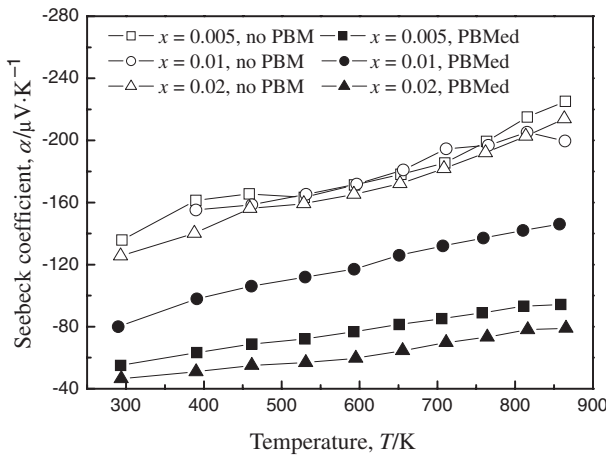
Figure 2 shows the SEM images of SCSed samples, considering the sample with an Al-doping amount of $x = 0.01$. Figures 2(a) and 2(b) show the samples directly after the SCS process; Fig. 2(c) shows the powder of the SCSed sample ground using the carnelian mortar and pestle; and Fig. 2(d) shows the powder obtained after the PBM process. As shown in Fig. 2, the SCSed sample was a friable agglomerate exhibiting a porous structure, and it could easily be ground into finer particles. The size of the crystal of the SCSed sample varied from nanosized crystals to those of the order of $3\ \mu\text{m}$. After the sample was ground using the carnelian mortar and pestle, the average particle size

decreased to $4\ \mu\text{m}$; however, the particle size distribution was not homogeneous, and a few large particle clusters were observed in the powder. After the PBM process, the particle size decreased to $1\text{--}2\ \mu\text{m}$, and the particle size distribution was homogeneous. This indicated that the PBM treatment could decrease and homogenize the particle size of the SCSed powders.

Figure 3 shows the SEM cross-section images of both no PBM and PBMed samples after SPS. As shown in the figure, the grain size of the no PBM samples ((a), (b), and (c)) is not homogeneous, which agrees with that shown in Fig. 2, and the samples are incompact. The PBMed samples ((d), (e), and (f)) have a relatively homogeneous grain size, and they are more compact than the no PBM samples. The relative densities of the sintered samples are listed in Table 1; the

Table 1 Characteristics of SCSed Al-doped ZnO.

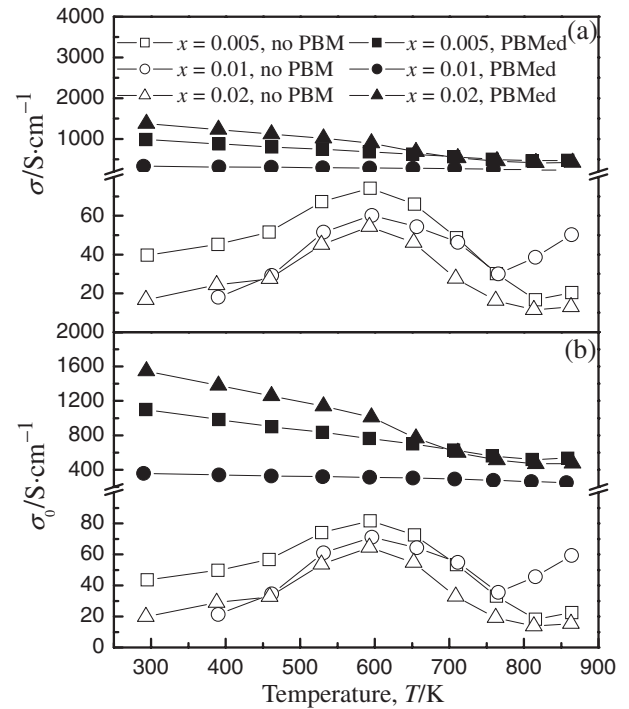
Experimental process	Sample names	Bulk densities (%(T.D.))	Lattice constants	
			<i>a</i> (nm)	<i>c</i> (nm)
Without PBM treatment before SPS	<i>x</i> = 0.005, no PBM	86.9	0.3248	0.5200
	<i>x</i> = 0.01, no PBM	89.1	0.3244	0.5206
	<i>x</i> = 0.02, no PBM	88.9	0.3248	0.5210
PBM before SPS	<i>x</i> = 0.005, PBMed	92.7	0.3233	0.5206
	<i>x</i> = 0.01, PBMed	92.9	0.3241	0.5203
	<i>x</i> = 0.02, PBMed	92.4	0.3241	0.5207

Fig. 4 Temperature dependence of Seebeck coefficient of spark plasma sintered $(\text{Zn}_{1-x}\text{Al}_x)\text{O}$ ($x = 0.005, 0.01, 0.02$).

lattice constants of the sintered samples are calculated by the XRD data and also listed in the table. The relative densities of the PBMed samples are 92–93%; they are higher than those of the no PBM samples because fine particles of the PBMed powders accelerated sintering, and dense samples were relatively easy to obtain. For both no PBM and PBMed samples, the value of the lattice constant *c* increased with the doping amount, except for the PBMed sample with $x = 0.01$; the reason for this phenomenon will be discussed later.

Figure 4 shows the dependence of the Seebeck coefficient of all the SCSed and spark plasma sintered Al-doped ZnO on temperature and doping amount. The Seebeck coefficient of all the samples was negative in the measurement temperature range, indicating that the samples were *n*-type materials; the absolute value of Seebeck coefficient increased with temperature.

Figure 5(a) shows the dependence of the experimental electrical conductivity on temperature and doping amount. As the densities of the samples were lower than 93% of the theoretical density, the effect of porosity on electrical conductivity was discussed. The effective conductivity of porous materials can be described by the Maxwell equation,²¹⁾ which is applicable to heterogeneous materials composed of spherical particles. Juretschke *et al.*²²⁾ proposed a mathematical model to interpret the relationship between the porosity and conductivity of ceramic materials based on Maxwell equation. Assuming that spherical pores are homogeneously distributed in dense materials, the relationship between relative conductivity and porosity can be expressed as

Fig. 5 Temperature dependence of (a) experimental electrical conductivity and (b) effective electrical conductivity of spark plasma sintered $(\text{Zn}_{1-x}\text{Al}_x)\text{O}$ ($x = 0.005, 0.01, 0.02$).

$$\frac{\sigma}{\sigma_0} = \frac{1 - \varepsilon}{1 + 0.5\varepsilon} \quad (4)$$

where σ and σ_0 are the experimental and effective electrical conductivities, respectively; and ε is the porosity of the material calculated by following equation:

$$\varepsilon = 1 - \frac{d}{d_0} \quad (5)$$

where d and d_0 are the experimental and theoretical densities, respectively. Therefore, the effective electrical conductivity of all samples was calculated using eqs. (4) and (5), and their plot against temperature is shown in Fig. 5(b). Comparing the PBMed and the no PBM samples, it was found that the former samples had higher electrical conductivity and smaller Seebeck coefficient (as shown in Fig. 4) than the latter samples. The reason for this phenomenon can be considered from two viewpoints. First, it was supposed that Al did not fully dissolve in the ZnO lattice during SCS, although the main phase of the samples directly after SCS process was Al-doped ZnO; the subsequent PBM process of PBMed samples caused alloying that lead to an increase in

the Al-concentration in the main phase of ZnO. Therefore, the Al concentration in the PBMed samples increased after PBM, which caused a decrease in the absolute value of the Seebeck coefficient and an increase in the electrical conductivity of the PBMed samples. In future studies, the effect of this aspect on the thermoelectric properties of Al-doped ZnO should be avoided by improving the SCS process by, for example, adjusting the amount of urea to control the amount of exhaust heat and optimizing the heating temperature of the SCS process. Second, according to a previous study, the spinel phase of ZnAl_2O_4 can be easily formed from Al_2O_3 and ZnO when the temperature is higher than 1073 K.²³⁾ In this study, although we did not detect any impurity phases by the XRD analysis, the impurity of ZnAl_2O_4 was probably formed at the grain boundaries of no PBM samples during SPS, because the powders formed in the absence of PBM were inhomogeneous, which deteriorated the sintering condition, thereby facilitating the synthesis of ZnAl_2O_4 . Therefore, the second phase of no PBM samples decreased the electrical conductivity. On the basis of the two viewpoints described above, PBMed samples had a higher electrical conductivity and a smaller Seebeck coefficient than those of no PBM samples.

Here, it should be mentioned that the electrical conductivity of no PBM samples first increased and then decreased with temperature. As the absolute value of the Seebeck coefficient of no PBM samples gradually increased with temperature, it showed that the carrier density did not change with measurement temperature for these samples. Therefore, the change in the temperature dependency on electrical conductivity was attributable to a change in the electron conduction mechanism, and the products exhibited a metallic behavior.

For no PBM samples doped with different amounts of Al, the Seebeck coefficient and electrical conductivity did not change considerably with an increase in the Al amount, and their values were very close to those of the reported ZnO samples.¹⁰⁾ For PBMed samples, the Seebeck coefficient decreased and electrical conductivity increased with the doping amount, except for the $x = 0.01$ sample. This indicated that PBM induced alloying of the samples in this study. The $x = 0.01$ PBMed sample had a different dependence of the thermoelectric properties on the doping amount, implying that this sample had a lower carrier density than that of the other two PBMed samples with $x = 0.005$ and $x = 0.02$. It was believed that the x value of this sample was lower than the expected x value of 0.01, which can also be verified by the lattice constant shown in Table 1. The c value of $x = 0.01$ PBMed sample was lower than that of the other two PBMed samples with $x = 0.005$ and $x = 0.02$, indicating that the sample was doped with a small amount of Al. Additionally, the fine particle size of the powders of PBMed samples improved the connection between the particles during sintering. Although voids were still detected in the SEM images of the sintered PBMed samples, the homogeneous distribution of the voids did not reduce electrical conductivity; this behavior was in agreement with that reported by Ohtaki *et al.*⁹⁾

Figure 6 shows the dependence of the power factor on the temperature and doping amount, calculated from the Seebeck

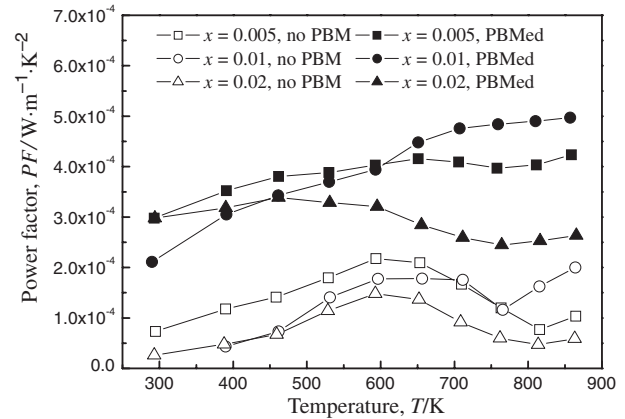


Fig. 6 Temperature dependence of power factor of spark plasma sintered ($\text{Zn}_{1-x}\text{Al}_x\text{O}$ ($x = 0.005, 0.01, 0.02$)).

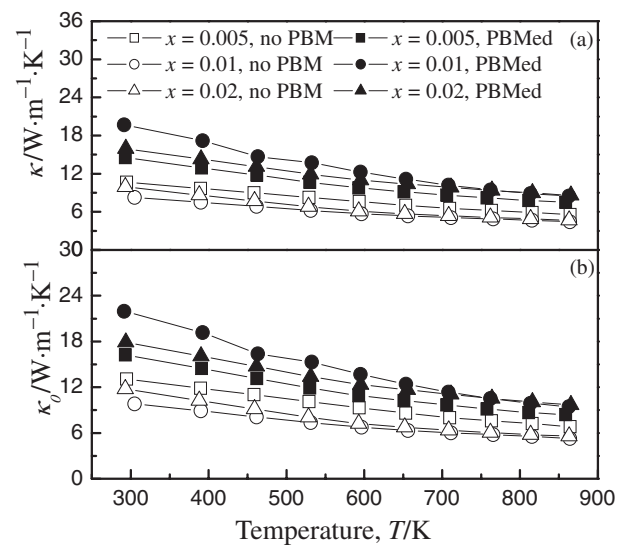


Fig. 7 Temperature dependence of (a) experimental thermal conductivity and (b) effective thermal conductivity of spark plasma sintered ($\text{Zn}_{1-x}\text{Al}_x\text{O}$ ($x = 0.005, 0.01, 0.02$)).

coefficient and electrical conductivity. Comparing the PBMed samples with the no PBM ones, it was observed that the former samples had a larger power factor than the latter samples in the experimental temperature range, which was caused by the high electrical conductivity. The results confirmed that the PBM treatment could improve the electrical properties of the SCSed Al-doped ZnO.

The experimental thermal conductivity of the Al-doped ZnO is shown in Fig. 7(a). Identical to the calculation of the effective electrical conductivity, the effective thermal conductivity κ_0 was calculated by the following equation:²⁴⁾

$$\frac{\kappa}{\kappa_0} = \frac{1 - \varepsilon}{1 + 0.5\varepsilon} \quad (6)$$

Figure 7(b) shows the dependence of the effective thermal conductivity on temperature. The effective thermal conductivity of Al-doped ZnO was higher than the experimental thermal conductivity. The thermal conductivity κ can be expressed by the following equation:

$$\kappa = \kappa_1 + \kappa_e \quad (7)$$

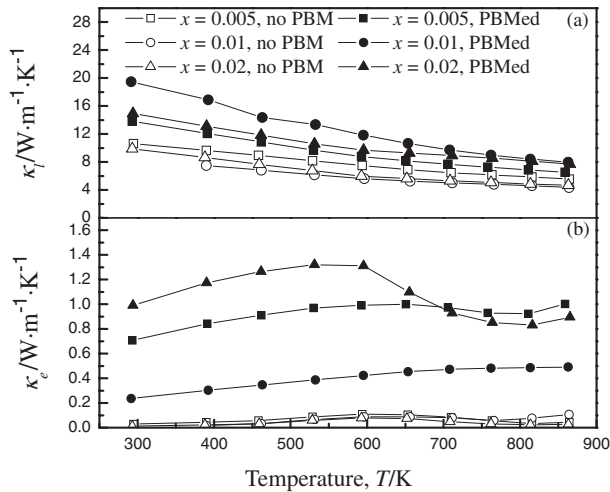


Fig. 8 Temperature dependence of (a) lattice thermal conductivity and (b) electronic thermal conductivity of spark plasma sintered $(\text{Zn}_{1-x}\text{Al}_x)\text{O}$ ($x = 0.005, 0.01, 0.02$).

where κ_l and κ_e are the lattice and electronic thermal conductivities, respectively. κ_e can be roughly estimated by the Wiedemann-Franz law as

$$\kappa_e = L\sigma T \quad (8)$$

where L is the Lorenz number. Therefore, the lattice thermal conductivity κ_l and the electronic thermal conductivity κ_e can be calculated using eqs. (7) and (8) with a Lorenz number of $2.45 \times 10^{-8} \text{W}\Omega\cdot\text{K}^{-2}$. The calculation results of κ_l and κ_e are shown in Figs. 8(a) and 8(b), respectively. As shown in Fig. 8, the thermal conductivity of the samples depends mainly on κ_l ; κ_e was a small fraction of the total thermal conductivity. The temperature dependence of κ_e was same as that of electrical conductivity, and κ_l decreased with temperature. The total thermal conductivity decreased with the increase of temperature; this was caused by a decrease in thermal diffusivity. In the experimental temperature range, the no PBM samples had a lower thermal conductivity than the PBMed samples, which was attributed to the presence of large voids and the formation of the second phase ZnAl_2O_4 at the grain boundary during the SPS of the no PBM samples. For both the no PBM and PBMed samples, the experimental thermal conductivity was in the range of $8.3\text{--}19.7 \text{W}\cdot\text{m}^{-1}\cdot\text{K}^{-1}$, and the effective thermal conductivity was in the range of $9.8\text{--}21.9 \text{W}\cdot\text{m}^{-1}\cdot\text{K}^{-1}$ at room temperature. These values were significantly lower than the reported values obtained by the conventional solid-state reaction method.^{8,25} The thermal conductivity was also lower than that reported by Cai *et al.*,¹⁸ obtained by the sol-gel method, and that reported by Ohtaki *et al.*,⁹ obtained by a method that generated a nanovoid structure. The low thermal conductivity obtained in our study is attributed to the following reasons: The small grain size of the samples and the presence of voids in them improved phonon scattering at grain boundaries, which decreased their electronic thermal conductivity and resulted in a relatively low total thermal conductivity of the samples in this study. This proved that SCS was an effective method for reducing thermal conductivity by synthesizing a product with a small crystal size.

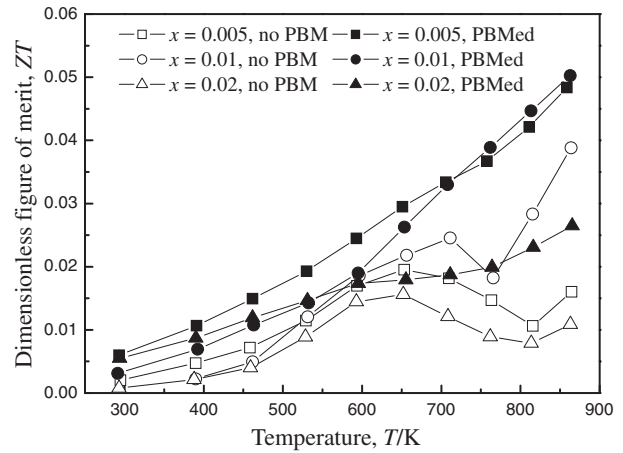


Fig. 9 Temperature dependence of dimensionless figure of merit ZT of spark plasma sintered $(\text{Zn}_{1-x}\text{Al}_x)\text{O}$ ($x = 0.005, 0.01, 0.02$).

Figure 9 shows the dependence of the dimensionless figure of merit ZT on temperature, calculated from the Seebeck coefficient, electrical conductivity, and thermal conductivity using eq. (1). Overall, ZT increased with temperature. Comparing the PBMed and no PBM samples, it was found that although the power factor of the PBMed samples was larger than that of the no PBMed ones, the difference in their ZT values was not significantly large because of a relatively high thermal conductivity of the PBMed samples. Among all samples, the PBMed sample with $x = 0.01$ had the maximum ZT value of 0.050 at the highest temperature of 863 K of our measurement temperature range. Although this ZT value was lower than the highest ZT value at 1250 K obtained from the reported data prepared by Ohtaki *et al.*,⁹ the thermoelectric properties were comparable to those of the reported data of the conventional solid-state reaction method, and ZT showed an increasing tendency at high temperature. In addition, ZT can possibly increase with an increase in the density of the sintered samples by optimizing the experimental conditions of SPS.

4. Conclusion

The thermoelectric properties of Al-doped ZnO, prepared by solution combustion synthesis using urea as fuel and sintered by spark plasma sintering, were investigated from room temperature to 865 K. The following results were obtained:

- (1) Al-doped ZnO with a small grain size was successfully synthesized by solution combustion synthesis.
- (2) A comparison of the PBMed samples with the no PBM samples showed that the former samples had a smaller Seebeck coefficient, higher electrical conductivity, and larger power factor than the latter samples in the experimental temperature range.
- (3) Under the experimental conditions, the PBMed samples had higher thermal conductivity than the no PBMed samples in the experimental temperature range. The thermal conductivity of all samples was in the range of $8.3\text{--}19.7 \text{W}\cdot\text{m}^{-1}\cdot\text{K}^{-1}$ at room temperature, which was significantly lower than that of the products synthesized by conventional synthesis methods.

- (4) As the temperature increased, ZT of all samples exhibited an increasing tendency. The PBMed sample with $x = 0.01$ had the highest ZT of 0.050 obtained at 863 K; ZT can possibly increase further with an increase in temperature and an improvement in the synthesis process.

The results showed that solution combustion synthesis was a promising method to synthesize Al-doped ZnO with low thermal conductivity for high temperature thermoelectric applications.

Acknowledgment

This study was partly supported by the 21st Century COE Program "Topological Science and Technology" from the Ministry of Education, Culture, Sports, Science and Technology of Japan. The authors are grateful to Mr. Kenji Ohkubo for his assistance in the thermal conductivity measurement.

REFERENCES

- 1) D. M. Rowe: *CRC Handbook of Thermoelectrics*, (CRC, Florida, 1995) pp. 1–5.
- 2) I. Terasaki, Y. Sasago and K. Uchinokura: *Phys. Rev. B* **56** (1997) 12685–12687.
- 3) T. Okuda, K. Nakanishi, S. Miyasaka and Y. Tokura: *Phys. Rev. B* **63** (2001) 113104.
- 4) L. Zhang, T. Tosho, N. Okinaka and T. Akiyama: *Mater. Trans.* **48** (2007) 2088–2093.
- 5) K. Koumoto, I. Terasaki and R. Funahashi: *MRS Bull.* **31** (2006) 206–210.
- 6) N. Okinaka and T. Akiyama: *Jpn. J. Appl. Phys.* **45** (2006) 7009–7010.
- 7) L. Zhang, T. Tosho, N. Okinaka and T. Akiyama: *Mater. Trans.* **48** (2007) 1079–1083.
- 8) M. Ohtaki, T. Tsubota, K. Eguchi and H. Arai: *J. Appl. Phys.* **79** (1996) 1816–1818.
- 9) M. Ohtaki and R. Hayashi: *Proc. 25th Int. Conf. on Thermoelectrics*, (2006) p. 276.
- 10) K. Park, J. K. Seong, Y. Kwon, S. Nahm and W. S. Cho: *Mater. Res. Bull.* **43** (2008) 54–61.
- 11) K. Park and K. Y. Ko: *J. Alloy. Compd.* **430** (2007) 200–204.
- 12) Y. Kinemuchi, C. Ito, H. Kaga, T. Aoki and K. Watari: *J. Mater. Res.* **22** (2007) 1942–1946.
- 13) K. Park, K. Y. Ko, W. S. Seo, W. S. Cho, J. G. Kim and J. Y. Kim: *J. Euro. Ceram. Soc.* **27** (2007) 813–817.
- 14) H. Kaga, Y. Kinemuchi, S. Tanaka, A. Makiya, Z. Kato, K. Uematsu and K. Watari: *Jpn. J. Appl. Phys.* **45** (2006) L1212–L1214.
- 15) K. H. Kim, S. H. Shim and K. B. Shi: *J. Am. Ceram. Soc.* **88** (2005) 628–632.
- 16) S. Katsuyama, Y. Takagi, M. Ito, K. Majima, H. Nagai, H. Sakai, K. Yoshimura and K. Kosuge: *J. Appl. Phys.* **92** (2002) 1391–1398.
- 17) Y. Tanaka, T. Ifuku, K. Tsuchida and A. Kato: *J. Mater. Sci. Lett.* **16** (1997) 155–157.
- 18) K. F. Cai, E. Müller, C. Drašar and A. Mroczek: *Mater. Sci. Eng. B* **104** (2003) 45–48.
- 19) T. Mimani and K. Patil: *Mater. Phys. Mech.* **4** (2001) 134–137.
- 20) A. S. Mukasyan, P. Epstein and P. Dinka: *Proc. Comb. Inst.* **31** (2007) 1789–1795.
- 21) J. C. Maxwell: *Treatise on Electricity and Magnetism*, (Oxford, 1673).
- 22) H. J. Juretscheke, R. Landauer and J. A. Swanson: *J. Appl. Phys.* **27** (1956) 838–839.
- 23) W. S. Hong, L. C. D. Jonghe, X. Yang and M. N. Rahaman: *J. Am. Ceram. Soc.* **78** (1995) 3217–3224.
- 24) A. Eucken: *Ceram. Abstr.* **11** (1932) 576.
- 25) T. Tsubota, M. Ohtaki, K. Eguchi and H. Arai: *J. Mater. Chem.* **7** (1997) 85–90.